Acknowledgements The Swedish 1-m Solar Telescope is operated on the island of La Palma by the Royal Swedish Academy of Sciences in the Spanish Observatorio del Roque de los Muchachos of the Instituto de Astrofisica de Canarias.

Competing interests statement The authors declare that they have no competing financial interests.

Correspondence and requests for materials should be addressed to D.K. (e-mail: dan@astro.su.se).

High-power terahertz radiation from relativistic electrons

G. L. Carr*, Michael C. Martin†, Wayne R. McKinney†, K. Jordan‡, George R. Neil‡ & G. P. Williams‡

** National Synchrotron Light Source, Brookhaven National Laboratory, Upton, New York 11973, USA*
† Advanced Light Source Division, Lawrence Berkeley National Laboratory, Berkeley, California 94720, USA
‡ Free Electron Laser Facility, Jefferson Laboratory, 12000 Jefferson Avenue, Newport News, Virginia 23606, USA

Terahertz (THz) radiation, which lies in the far-infrared region, is at the interface of electronics and photonics. Narrow-band THz radiation can be produced by free-electron lasers[1] and fast diodes[2,3]. Broadband THz radiation can be produced by thermal sources and, more recently, by table-top laser-driven sources[4–6] and by short electron bunches in accelerators[7], but so far only with low power. Here we report calculations and measurements that confirm the production of high-power broadband THz radiation from subpicosecond electron bunches in an accelerator. The average power is nearly 20 watts, several orders of magnitude higher than any existing source, which could enable various new applications. In particular, many materials have distinct absorptive and dispersive properties in this spectral range, so that THz imaging could reveal interesting features. For example, it would be possible to image the distribution of specific proteins or water in tissue, or buried metal layers in semiconductors[8,9]; the present source would allow full-field, real-time capture of such images. High peak and average power THz sources are also critical in driving new nonlinear phenomena and for pump–probe studies of dynamical properties of materials[10,11].

The THz region (1 THz ≈ 33 cm^{-1} or 4 meV) lies in the far-infrared spectral range where conventional thermal sources are very weak. For example, a blackbody source at 2,000 K provides less than 1 μW per cm^{-1} of spectral power density for a typical spectroscopy application. Whereas narrowband sources have been available using free-electron laser (FEL) technology[1,12], a significant advance in broadband THz sources has occurred over the past decade with the advent of coherent THz radiation emission from photocarriers in biased semiconductors. Table-top systems using optical rectification of femtosecond lasers either at high repetition rates[5] or high peak power[6] are routinely available.

The present work describes a different process for producing coherent THz radiation by accelerated electrons. Like the method described in ref. 5, the process begins with pulsed laser excitation in GaAs, but makes use of photoemission to produce bunches of free electrons in space. Using the energy-recovered linac (ERL) at the Jefferson Laboratory FEL[13], very short electron bunches (~500 fs) are brought to relativistic energies (~40 MeV) in a linac and then transversely accelerated by a magnetic field to produce the desired THz emission as synchrotron radiation. This unique accelerator is capable of a running with a relatively high average beam current (up to 5 mA). Like the THz emitter described in ref. 5, the electrons experience a common acceleration. If the electron bunch dimensions are small (in particular, the bunch length is less than the wavelength of observation), we again obtain a multiparticle coherent enhancement[14,15]. Such coherent synchrotron radiation has been observed from electrons accelerated in linacs[7,16–18], from compact waveguide FELs[19] and from magnetic undulators[19–21]. Coherent THz radiation has been discussed, and observed from electron bunches in storage rings[22–25], but not yet stably enough for use as a light source. Active programmes to study THz radiation from linacs or storage rings are underway at BESSY II (Berliner Elektronenspeicherring-Gesellschaft für Synchrotronstrahlung; www.bessy.de) and DESY (Deutsches Elektronen Synchrotron) in Germany, and at Brookhaven National Laboratory and Lawrence Berkeley National Laboratory in the USA. In addition, programmes are underway at ENEA-Frascati to generate broadband THz radiation by exploiting the distinctive properties of waveguide FELs which arise when the electron velocity is close to the group velocity of the wave packet[26]. Some linacs can create very short bunches (<1 ps) and produce coherent radiation up to a few THz, but most are limited to repetition rates of a few Hz, so the average power is quite low. The repetition rate for storage rings is of the order of 100 MHz, but the electron bunches are significantly longer (~100 ps) owing to longitudinal damping through synchrotron radiation emission. Thus the emission is limited to the very low frequency regime (far-infrared), or arises from instabilities that briefly modify the bunch shape.

Our ERL accelerator system overcomes some of the limitations of conventional linacs and storage rings. Electron bunches as short as ~500 fs are produced by the standard technique of energy modulation (chirping) followed by compression in the dispersive region of a magnetic chicane[27]. The time taken for an electron bunch to pass through the accelerator is less than 1 μs; thus longitudinal damping is negligible. But unlike most linacs, our system operates at a very high repetition rate (up to 75 MHz) by using superconducting radio frequency cavities and recovering the energy of the spent electron bunches[13] so that the average current is orders of magnitude higher than in conventional linacs.

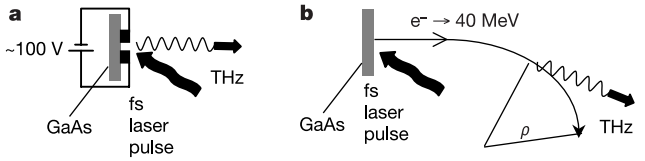

Figure 1 Comparison between coherent THz radiation generated by an 80-MHz conventional laser-driven THz source (**a**) and the relativistic source described here (**b**). In **a**, the photo-induced carriers immediately experience a force from the bias field (~100 V across a 100 μm gap) of ~10^6 V m^{-1}, which results in an acceleration of 10^{17} m s^{-2}. The entire process is completed in less than 1 ps, resulting in spectral content up to a few THz. In **b**, approximately the same number of charge carriers are brought to a relativistic energy of >10 MeV in a linac, after which a magnetic field bends their path into a circle of radius $\rho = 1$ m, resulting in an acceleration $c^2/\rho = 10^{17}$ m s^{-2}, the same as for **a**. An observer of **b** would also detect a brief pulse of electromagnetic radiation as an electron bunch passed by. But in this case, two factors control the pulse duration; one is the bunch length, and the other is the time for the relativistically compressed acceleration field from each electron to sweep past. The latter is given approximately by[28] $\delta t = 4\rho/(3\gamma^3 c)$, and determines the spectral range emitted by each electron. The bunch length determines the spectral range over which the coherent enhancement occurs. For an electron energy of 10 MeV ($\gamma = 21$), and with $\rho = 1$ m, we obtain a δt of about 500 fs, which is comparable to the bunch length. The resulting spectral content extends up to about 1 THz, the same spectral range as for **a**. With all factors except γ the same, we see from equation (1) that the power radiated by a relativistic electron exceeds that from a conventional THz emitter by a factor of $\gamma^4 = 21^4 = 2 \times 10^5$.

We now examine how our system generates THz power many orders of magnitude more efficiently than a more conventional (non-relativistic) THz source[5]. The diagram in Fig. 1 shows the two processes for comparison. In both cases, a short light pulse from a mode-locked laser strikes a GaAs wafer, generating charge carriers. Thus the number of radiating charges should be comparable (same order of magnitude) for both cases. We can therefore compare the power produced per electron, and use Larmor's formula[28] for the radiated power P. In c.g.s. units it takes the form

$$P = \frac{2e^2a^2}{3c^3}\gamma^4 \tag{1}$$

where e is the charge, a is the acceleration, c the speed of light and γ is the ratio of the mass of the electron to its rest mass. With all factors except γ the same, we see from equation (1) that for our case the power radiated by a relativistic electron exceeds that from a conventional THz emitter by a factor of $\gamma^4 = 21^4 = 2\times10^5$. In practice, the electron energy can be significantly larger, but this simply adds intensity at higher frequencies and leaves the low-frequency (THz) intensity essentially unchanged.

We mention again that both cases benefit from multiparticle coherent emission, as many radiating charges are contained physically within one period of the emitted THz radiation. Theoretically, the more general expression for the power emitted by an electron bunch, as a function of frequency (ω) and solid angle (Ω), is derived by extending the classical theory of electrodynamics[28] for a single electron, to a system of N electrons, thus[14,15]:

$$\frac{\mathrm{d}^2I}{\mathrm{d}\omega\ \mathrm{d}\Omega} = [N[1-f(\omega)] + N^2 f(\omega)] \times \frac{e^2\omega^2}{4\pi^2 c}\left|\int_{-\infty}^{\infty} \hat{n}\times(\boldsymbol{\beta}\times\hat{\mathbf{n}})e^{\mathrm{i}\omega\left(t-\frac{\hat{n}\cdot\mathbf{r}(t)}{c}\right)}\,\mathrm{d}t\right|^2 \tag{2}$$

where β is the ratio of the velocity of the particle bunch to the velocity of light, $\hat{n}$ is a unit vector along the direction of propagation (to the observer), $\mathbf{r}(t)$ is the location of the electron bunch centre, and N is the number of particles in the bunch. The term $N^2f(\omega)$ represents the coherent enhancement, and includes the form factor $f(\omega)$ which is the Fourier transform of the normalized longitudinal particle distribution within the bunch; that is,

$$f(\omega) = \left|\int_{-\infty}^{\infty} e^{iw\hat{\mathbf{n}}\cdot\mathbf{z}/c}S(z)\,\mathrm{d}z\right|^2 \tag{3}$$

where $S(z)$ is the distribution function for particles in the bunch, measured relative to the bunch centre.

A practical solution to the second major term in equation (2) has been presented in ref. 29. For the present calculations (Fig. 2), we assume 40-MeV electron bunches each carrying 100 pC of charge, passing through a 1-m-radius bend at a 37.4-MHz repetition rate. For simplicity, we assume that each bunch has a gaussian particle distribution of width σ, yielding a gaussian form factor:

$$f(\omega) = e^{-\left(\frac{\omega\sigma}{c}\right)^2} = e^{-4\pi^2\sigma^2\left(\frac{1}{\lambda}\right)^2} \tag{4}$$

where λ is the wavelength of the light at frequency ω. The bunches are not strictly gaussian in practice, but this approximation is useful for estimating the overall power and spectral content. The electron beam had an r.m.s. width and height of 1 mm. Given a natural emission angle, $1.66(\lambda/\rho)^{1/3}$ of 0.11 rad at 1 THz, where ρ is the bending radius, the diffraction-defined source size was of the order of the electron beam size, and the emitted radiation had an extremely high degree of transverse spatial coherence. This allows for interferometry by a simple form of wavefront division[30].

In our experiments using the ERL THz source, the electrons were generated using the frequency-doubled output of a Nd:YLF laser (model Antares, made by Coherent) operating at, or a sub-multiple of, 74.8 MHz, and with an average power of a few watts. Light of wavelength 530 nm was incident on a negative electron affinity Cs-coated GaAs cathode. The resulting photoelectrons were accelerated using a d.c. voltage of 300 kV into a superconducting linac, and accelerated to an energy of 40 MeV. Although the electrons are initially emitted from the cathode with a pulse length of ~40 ps full-width at half-maximum, they become tightly bunched in the accelerator to pulse lengths less than 1 ps. After passing through the accelerator system, the electrons are decelerated in the same linac to an energy of 10 MeV before reaching the beam dump, thus recovering most of the beam energy. This energy recovery allows average current of up to 5 mA and electron bunches containing up to 135 pC, using an r.f. system nominally capable of accelerating only 1.1 mA beam current.

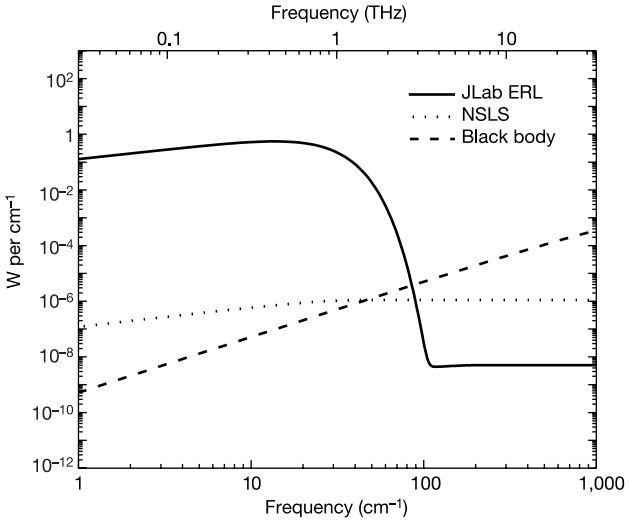

Figure 2 Calculations of the average power emitted by a 10-mm^2 thermal source at 2,000 K (dashed line), the NSLS VUV ring at Brookhaven National Laboratory (dotted line), and the Jefferson Laboratory (JLab) ERL (solid line). The NSLS was calculated for a stored current of 800 mA and 90 mrad (vertical) by 90 mrad (horizontal) collection. The JLab ERL was calculated for 500-fs FWHM, 100-pC bunches at a repetition rate of 37.4 MHz (for an average current of 3.7 mA) and 60 mrad (vertical) by 60 mrad (horizontal) collection. The increased power of the JLab ERL in the THz range is clear. We also note that the calculation assumes that the ERL has an average current of 3.7 mA compared with 800 mA at the NSLS, Brookhaven, so that in the incoherent regime the NSLS has 800/3.7 = 216 times the power per cm^{-1}. However, in the THz spectral range (where the JLab ERL emits coherently and the NSLS does not) the ERL has 3.9×10^6 times the power of the NSLS.

The ERL THz radiation was extracted from a dipole magnet of 1 m bending radius immediately before the FEL cavity, the latter being unimportant for these experiments. For the total power measurements, the radiation left the accelerator vacuum chamber through a 10-mm-aperture diamond window subtending an angle of 20×20 mrad relative to the source point. The emerging beam was focused onto a calibrated $LiTaO_3$ pyroelectric detector, calibrated with equipment traceable to NIST. This detector had a nearly flat response (J25, Molectron) out to THz wavelengths owing to a black organic coating, and a nominal responsivity of 8.83 V J^{-1} (±2%).

The spectral content of the ERL THz radiation was analysed using a rapid-scan Michelson interferometer (Nexus 670, Nicolet) with a silicon beamsplitter. The light was detected using a 4.2 K bolometer (Infrared Laboratories) with a 2 mm × 2 mm boron-doped Si composite element, fed from a 12-mm-diameter f/4 Winston cone. It was fitted with a black polyethylene filter to ensure no radiation above 600 cm^{-1} was detected. The diamond window on the accelerator was replaced by a larger crystal-quartz window to

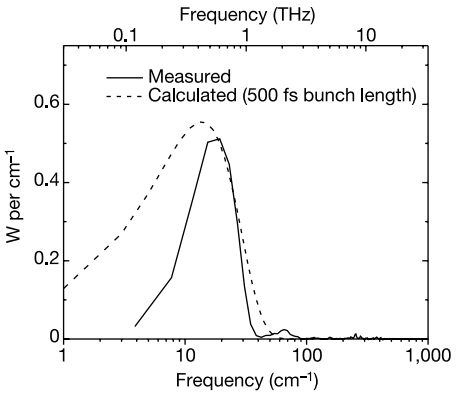

Figure 3 Comparison between measured (solid line) and calculated (dashed line) THz spectral intensity. We also show a curve calculated for a bunch length of 500 fs, which is reasonable for the machine operating under the conditions of the experiment. We have scaled the data to fit the theory on the basis of the absolute power measurements. The spectral onset of the super-radiant enhancement on the high-frequency side is clearly seen, with the shape matching the theoretical prediction. Note that there is a severe discrepancy on the lower-frequency side owing to diffraction effects. This can be understood in the following way. At 10 cm^{-1} and with an *f*/17 beam, the diffraction-limited source size is 17 mm, almost the same as the extraction optics. At 1 cm^{-1}, the diffraction-limited source size would, at 170 mm, be more than 3 times larger than the vacuum chamber containing the electron beam. Note also the additional peak at 60 cm^{-1}, which we attribute to the non-gaussian nature of the electron bunch. As we measured the intensity, not field, of the emitted light, we were unable to determine uniquely the electron density distributions, but this might be possible in future experiments using coherent detection.

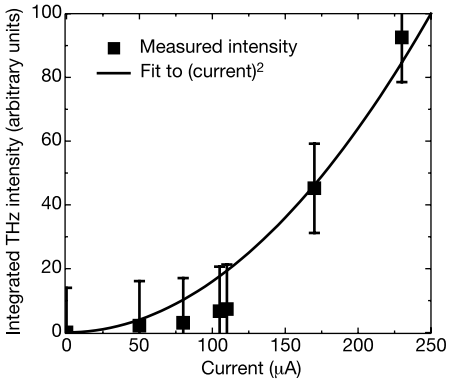

Figure 4 Measured THz intensity as a function of beam current (square symbols), showing the quadratic dependence expected for coherent emission (solid line). We note that in our experiments we were able to observe considerable changes in spectral weight depending on operating conditions, and we were able to enhance certain spectral regions in a controlled way via the machine parameters. Thus the electron bunch distributions were not purely gaussian. This accounts for the large error bars.

increase the energy collection to 60 × 60 mrad. A spherical mirror of 80 cm focal length produced a 48-mm-diameter collimated beam compatible with the interferometer optics. A switching mirror allowed a remote choice of source, namely the THz energy from the accelerator, or a $T = 1{,}300$ K thermal reference source (see below).

For the spectroscopy experiments, the analysis and detection system did not have sufficient dynamic range to cover the seven decades in power difference between the two sources. But as mentioned earlier, the ERL THz source could be run at a precisely defined lower repetition rate. In this way we could reduce the average power without changing the spectral content. We chose to make measurements at 584 kHz, instead of 37.4 MHz, and at a charge per bunch of 34 pC instead of 100 pC, thereby reducing the ERL THz power by a factor of $\{(34\times10^6)/(584\times10^3)\}\times(100/34)^2$, or approximately 550.

We have another reference point for determining the absolute power, as we were able to switch sources from the ERL THz emission port to a 1,300 K thermal source (the spectrometer's standard 'globar' source). This allowed us to measure the relative power using the same spectrometer and detection system. At a frequency of 12 cm^{-1} we obtained a ratio of intensity from the ERL THz source to that of the globar of 2×10^4. To compare with the calculation, we multiply the results for the THz source by the reduction factor of 550, as discussed earlier. This implies a measured advantage of the ERL THz source over the globar of 10^7. The calculation predicts an enhancement of $0.6/(6\times10^{-8}) = 10^7$. The data are shown in Fig. 3, and the result affirms the large ERL THz power. The level of agreement is somewhat surprising, as our simple arguments have ignored diffraction and detection efficiency. In fact, owing to uncertainties in the absorbance of the detector coating in the THz region, the reported data place a lower bound on the power measurement.

One additional property of super-radiant emission from electrons is the dependence of the intensity on the square of the number of particles per bunch from equation (2). In Fig. 4 we plot the integrated intensity as a function of bunch charge, which shows good agreement with the theoretical N^2 curve.

Finally, we measured the polarization of the emitted THz radiation. The intensity ratio for the horizontal to vertical polarization components is 3 for synchrotron radiation in the long-wavelength limit. This assumes full collection of the emitted radiation. We note that the dominant intensity is near 30 cm^{-1}, which has a natural opening angle of 86 mrad. As the emission pattern is 'clipped' by the 60-mrad collection optics, the calculated ratio is expected to be higher, approaching a value of 6. Using a wire-grid polarizer placed between the Michelson modulator and the detector, we measured a ratio of 5 and consider this to be good agreement.

We have produced broadband, high-brightness, THz radiation with close to 1 W per cm^{-1} of average spectral power density into the diffraction limit, and peak spectral power densities about 10^4 times higher than this. However, one area of concern remains—the question of timing jitter and current fluctuations, and their effect on coherent detection and signal to noise ratio. As energy-recovery linac THz sources are being considered for other applications, some of which involve timing, it is important to evaluate timing jitter and current fluctuations. We have made preliminary measurements using a frequency analyser, and plan further detailed studies. □

Received 12 March; accepted 30 September 2002; doi:10.1038/nature01175.

1. Ramian, G. The new UCSB free-electron lasers. *Nucl. Instrum. Methods Phys. Res. A* **318,** 225–229 (1992).
2. Porterfield, D. W., Crowe, T. W., Bradley, R. F. & Erickson, N. R. A high-power, fixed-tuned, millimeter-wave balanced frequency doubler. *IEEE Trans. Microwave Theory Techn.* **MTT-47,** 419–425 (1999).
3. Siegel, P. H. Terahertz technology. *IEEE Trans. Microwave Theory Techn.* **MTT-50,** 910–928 (2002).
4. Auston, D. H., Cheung, K. P., Valdmanis, J. A. & Kleinman, D. A. Cherenkov radiation from femtosecond optical pulses in electrooptic media. *Phys. Rev. Lett.* **53,** 1555–1558 (1984).
5. Bonvalet, A., Joffre, M., Martin, J. L. & Migus, A. Generation of ultrabroadband femtosecond pulses in the mid-infrared by optical rectification of 15 fs light pulses at 100 MHz repetition rate. *Appl. Phys. Lett.* **67,** 2907–2909 (1995).
6. You, D., Jones, R. R., Bucksbaum, P. H. & Dykaar, D. R. Generation of high-power sub-single-cycle 500-fs electromagnetic pulses. *Opt. Lett.* **18,** 290–292 (1993).
7. Nakazato, T. *et al.* Observation of coherent synchrotron radiation. *Phys. Rev. Lett.* **63,** 1245–1248 (1989).
8. Chen, Q. & Zhang, X.-C. *Ultrafast Laser Technology and Applications* (eds Fermann, M. E., Galvanauskas, A. & Sucha, G.) 521–572 (Marcel Dekker, New York, 2001).
9. Zhang, X.-C. in *Compound Optoelectronic Materials and Devices* 69–80 (1995).
10. Cole, B. E., Williams, J. B. & King, B. T. Coherent manipulation of semiconductor quantum bits with terahertz radiation. *Nature* **410,** 60–63 (2001).
11. Huber, R. *et al.* How many-particle interactions develop after ultrafast excitation of an electron–hole plasma. *Nature* **414,** 286–289 (2001).

12. Winnerl, S. *et al.* Frequency doubling and tripling of terahertz radiation in a GaAs/AlAs superlattice due to frequency modulation of Bloch oscillations. *Appl. Phys. Lett.* **77,** 1259–1261 (2000).
13. Neil, G. R. *et al.* Sustained kilowatt lasing in a free-electron laser with same cell energy recovery. *Phys. Rev. Lett.* **84,** 662–665 (2000).
14. Nodvick, S. & Saxon, D. S. Suppression of coherent radiation by electrons in a synchrotron. *Phys. Rev.* **96,** 180–184 (1954).
15. Hirschmugl, C. J., Sagurton, M. & Williams, G. P. Multiparticle coherence calculations for synchrotron radiation emission. *Phys. Rev. A* **44,** 1316–1320 (1991).
16. Happek, U., Blum, E. B. & Sievers, A. J. Observation of coherent transition radiation. *Phys. Rev. Lett.* **67,** 2962–2965 (1991).
17. Wang, D. X., Krafft, G. A. & Sinclair, C. K. Measurement of femtosecond electron bunches using a rf zero-phasing method. *Phys. Rev. E* **57,** 2283–2286 (1998).
18. Lihn, H.-C., Kung, P., Settakorn, C. & Wiedemann, H. Observation of stimulated transition radiation. *Phys. Rev. Lett.* **76,** 4163–4166 (1996).
19. Doria, A., Bartolini, R., Feinstein, J., Gallerano, G. P. & Pantell, R. H. Coherent emission and gain from a bunched electron beam. *IEEE J. Quant. Electron.* **QE-29,** 1428–1436 (1993).
20. Jaroszynsky, D. A., Bakker, R. J., van der Geer, C. A. J., Oepts, D. & van Amersfoort, P. W. Coherent start-up of an infrared free electron laser. *Phys. Rev. Lett.* **71,** 3798–3801 (1993).
21. Berryman, K. W., Crosson, E. R., Ricci, K. N. & Smith, T. I. Coherent spontaneous radiation from highly bunched electron beams. *Nucl. Instrum. Methods Phys. Res. A* **375,** 526–529 (1996).
22. Tamada, H., Tsutsui, H., Shimoda, K. & Mima, K. Features of the compact photon storage ring. *Nucl. Instrum. Methods A* **331,** 566–571 (1993).
23. Andersson, A., Johnson, M. S. & Nelander, B. Coherent synchrotron radiation in the far infrared from a 1-mm electron bunch. *Opt. Eng.* **39,** 3099–3105 (2000).
24. Arp, U. *et al.* Spontaneous coherent microwave emission and the sawtooth instability in a compact storage ring. *Phys. Rev. Spec. Topics Accelerat. Beams* **4,** 54401 (2001).
25. Carr, G. L. *et al.* Observation of coherent synchrotron radiation from the NSLS VUV ring. *Nucl. Instrum. Methods A* **463,** 387–392 (2001).
26. Giovenale, E. *et al.* Longitudinal phase-space manipulation: a device to enhance the coherent emission from an RF modulated electron beam. *Nucl. Instrum. Methods* **437,** 128–133 (1999).
27. Yu, L. H., Johnson, E., Li, D. & Umstadter, D. Femtosecond free-electron laser by chirped pulse amplification. *Phys. Rev. E* **49,** 4480–4486 (1994).
28. Jackson, J. D. *Classical Electrodynamics* (Wiley, New York, 1975).
29. Hulbert, S. L. & Williams, G. P. *Handbook of Optics: Classical, Vision, and X-Ray Optics* Vol. III, *Synchrotron Radiation Sources*, 2nd edn (eds Bass, M., Enoch, J. M., Van Stryland, E. W. & Wolfe, W. L.) 32.1–32.20 (McGraw-Hill, New York, 2001).
30. Moeller, K. D. *et al.* . *Appl. Opt.* **30,** 4297–4301 (1991).

Acknowledgements We thank our colleagues for their help and support, which were essential for these experiments. This work was supported primarily by the US Department of Energy. The Jefferson Laboratory FEL is supported by the Office of Naval Research, the Air Force Research Laboratory, the Commonwealth of Virginia and the Laser Processing Consortium.

Competing interests statement The authors declare that they have no competing financial interests.

Correspondence and requests for materials should be addressed to G.P.W. (e-mail: gwyn@mailaps.org).

Ferromagnetism of a graphite nodule from the Canyon Diablo meteorite

J. M. D. Coey*, M. Venkatesan*, C. B. Fitzgerald*, A. P. Douvalis* & I. S. Sanders†

* *Physics Department,* † *Geology Department, Trinity College, Dublin 2, Ireland*

There are recent reports of weak ferromagnetism in graphite[1,2] and synthetic carbon materials[3] such as rhombohedral C_{60} (ref. 4), as well as a theoretical prediction of a ferromagnetic instability in graphene sheets[5]. With very small ferromagnetic signals, it is difficult to be certain that the origin is intrinsic, rather than due to minute concentrations of iron-rich impurities. Here we take a different experimental approach to study ferromagnetism in graphitic materials, by making use of meteoritic graphite, which is strongly ferromagnetic at room temperature. We examined ten samples of extraterrestrial graphite from a nodule in the Canyon Diablo meteorite. Graphite is the major phase in every sample, but there are minor amounts of magnetite, kamacite, akaganéite, and other phases. By analysing the phase composition of a series of samples, we find that these iron-rich minerals can only account for about two-thirds of the observed magnetization. The remainder is somehow associated with graphite, corresponding to an average magnetization of 0.05 Bohr magnetons per carbon atom. The magnetic ordering temperature is near 570 K. We suggest that the ferromagnetism is a magnetic proximity effect induced at the interface with magnetite or kamacite inclusions.

Many carbon-based ferromagnets order magnetically below 20 K (refs 6, 7), but the recent study[4] of polymerized rhombohedral C_{60} found a Curie temperature, T_C, of about 500 K and a spontaneous magnetization $\sigma_s = 0.09\,A\,m^2\,kg^{-1}$. An extensive study of graphite samples of different provenance[1] suggested an intrinsic origin for the ferromagnetism, although the spontaneous magnetization at room temperature did not exceed $0.003\,A\,m^2\,kg^{-1}$. Another intriguing report is that ferromagnetism with $\sigma_s = 0.02\,A\,m^2\,kg^{-1}$ may coexist with superconductivity in the graphite–sulphur system[8]. To put the weakness of the ferromagnetism in perspective, carbon with a ferromagnetic moment of 1 Bohr magneton (μ_B) per atom would have $\sigma_s = 465\,A\,m^2\,kg^{-1}$, and a corresponding polarization $J_S = 1.2$ T. It seems that either a tiny fraction of the carbon atoms participate in the magnetism of these materials, or the carbon moment is remarkably weak ($\sim 10^{-4}\,\mu_B$). An exception is amorphous carbon prepared by direct pyrolysis[3], which in one case[9] was reported to have a room-temperature magnetization of $9.2\,A\,m^2\,kg^{-1}$, or $0.02\,\mu_B$ per carbon. We have reproduced this result, but find iron in the form of micrometre-sized oxide particles dispersed throughout the carbon.

The impact some 50,000 years ago of the 50,000-tonne Canyon Diablo meteorite at a relative velocity of about $20\,km\,s^{-1}$ was a cataclysmic event, which created a crater of diameter 1.3 km in the Arizona desert. Canyon Diablo is classified as a silicate-bearing IAB iron[10,11]. The origin of this group is puzzling, but it may have involved catastrophic mixing of the molten iron core of an asteroid in a collision with a chondritic body in the first few million years of

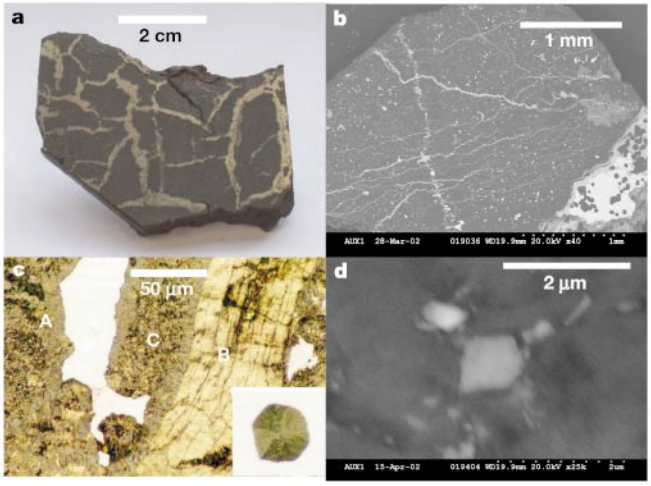

Figure 1 The Canyon Diablo graphite nodule at increasing magnifications. **a**, Cut and polished section of the whole nodule, showing interconnecting veins of kamacite ($Fe_{94}Ni_6$) in the graphite matrix. **b**, Backscattered electron image of graphite lightly peppered with tiny nuggets of kamacite (bright flecks) and traversed by thin, subparallel veins of oxidized iron (pale grey). A partially oxidized kamacite vein (bottom right) contains black inclusions of cliftonite[18], a variety of graphite comprising radiating clusters of crystallites that appear to have grown by exsolution from carbon-rich metal on cooling. **c**, Reflected polarized light image of polished graphite showing three distinct forms: A, a continuous border of cliftonite surrounding an embayed nugget of kamacite, B, a large buckled plate of graphite (pale gold), and C, a poorly polished, felted mass of graphite crystallites. Inset, a cliftonite inclusion in metal at the same scale. **d**, Backscattered image of graphite with embedded iron-rich inclusions, possibly magnetite, down to 50 nm in size.

